

Pre-Clinical Changes Observed by Magnetic Resonance Imaging in a Hamster Model of Transmissible Spongiform Encephalopathy: a Potential Biomarker of Prion Infection

Richard. S. Baydack^{1,2,3}, Eilean J. McKenzie^{1,3}, Catherine Robertson^{1,4}, Stephanie. A. Booth^{1,4}, Mike Jackson³ and Timothy F. Booth^{1,2*}

¹Department of Medical Microbiology 745 Bannatyne Avenue, University of Manitoba, Winnipeg, Manitoba, R3E 0J9 Canada

²Viral Diseases Division, National Microbiology Laboratory, Public Health Agency of Canada, Canadian Science Centre for Human and Animal Health, 1015 Arlington St., Winnipeg, Manitoba, R3E 3R2, Canada

³National Research Council Canada, Institute for Biodiagnostics 435 Ellice Avenue Winnipeg Manitoba, R3B 1Y6

⁴Molecular Pathobiology, National Microbiology Laboratory, Public Health Agency of Canada, Canadian Science Centre for Human and Animal Health 1015 Arlington St. Winnipeg, Manitoba, R3E 3R2, Canada

Abstract

The objective of the study was to develop a model for the diagnosis of prion diseases in live animals, using magnetic resonance imaging (MRI). Hamsters experimentally infected with the 263K strain of scrapie were imaged periodically during the course of prion infection. Changes in the brain, particularly the hippocampus, were observed during the first quarter of the incubation period. These changes included an increase in T_2 relaxation time and apparent diffusion coefficient (ADC), indicative of an increase in the water content of tissues. These changes were apparent well before the appearance of clinical symptoms, and did not correlate with the typical histological changes characteristic of prion disease, (vacuolation, accumulation of PrP protein, gliosis) suggesting that the changes are caused by a progressive accumulation of fluid. This oedema may be a novel early marker of prion disease, and could play a role in pathogenesis.

Introduction

Transmissible spongiform encephalopathies (TSEs), or prion diseases, are a group of invariably fatal neurodegenerative diseases of both humans and animals caused, in whole or in part, by an abnormally-folded form of the normal cellular protein PrP [1]. The normal form of this protein, known as PrP^C, undergoes a conformational change during which it acquires a significant amount of β -sheet [2,3], producing the pathological form, PrP^{Sc}, which is partially protease resistant and insoluble [2,4]. Prion diseases exist in genetic, sporadic, and acquired forms, all of which are transmissible [5]. The most common human prion disease is Creutzfeldt-Jakob Disease (CJD), the variant form (vCJD) of which is likely acquired through ingestion of beef from Bovine Spongiform Encephalopathy (BSE) infected cattle [1,6,7]. Other prion diseases include scrapie of sheep and goats, and Chronic Wasting Disease (CWD) of deer and elk in North America.

For research, rodent adapted prion strains, such as the 263K strain of scrapie in Syrian golden hamsters, are useful models due to the relatively short incubation period of 68-71 days following intra-cerebral infection [8-10]. Prion diseases are characterized by the deposition of PrP^{Sc}, the appearance of vacuoles, and gliosis in the brain [5]. Different strains can be distinguished by the distributions of these histological markers in a given host. However, the unequivocal diagnosis of most prion diseases requires the post-mortem collection of central nervous system tissue, either for histological examination or Western blot analysis.

Since changes in soft tissues like the brain can be detected by magnetic resonance imaging (MRI), this method has been used to examine patients suspected of having CJD or other prion diseases. MR image abnormalities that have been reported include: increased signal on T_2 -weighted images in the basal ganglia [11,12], caudate nuclei and putamina [13], and cerebral cortex [11]; increased signal on T_1 -weighted images in the globus pallidus [14]; and increased signal on diffusion-weighted images in the cerebral cortex [15,16], basal ganglia [16], and striatum [15]. In some cases, MR image abnormalities were compared to histological changes evident in tissues collected upon

death. High signal intensity on diffusion-weighted [11,17], and T_2 -weighted [11] images correlated with a high degree of spongiform change. In experimentally-infected rodents, increased signal intensity on T_2 -weighted images correlated with gliosis [18,19] or PrP^{Sc} deposition [19], while vacuolation correlated with decreased signal intensity [18]. Only one previous report has described pre-clinical changes, and they were observed late in the pre-clinical stage of disease [19]. We report here, for the first time, the observation by MRI of changes that occur very early following the infection of hamsters with the 263K strain of scrapie, during the first quarter of the incubation period. These changes involve increases in T_2 relaxation time and apparent diffusion coefficient (ADC), and were evident well before the appearance of either clinical symptoms or the typical histological changes characteristic of prion disease. We conclude that the early MR abnormalities observed are the result of the progressive accumulation of fluid in the hippocampus, and that observation of these changes may be useful as a novel early biomarker of prion disease pathogenesis.

Results

Magnetic Resonance Imaging - T_2 Changes in Scrapie-Infected Hamsters

Syrian golden hamsters were inoculated intra-cerebrally with 263K

*Corresponding author: Tim F Booth, National Microbiology Laboratory Winnipeg, Manitoba Canada, E-mail: tim.booth@phac-aspc.gc.ca

Received October 12, 2011; Accepted November 15, 2011; Published November 21, 2011

Citation: Baydack RS, McKenzie EJ, Robertson C, Booth SA, Jackson M, et al. (2011) Pre-Clinical Changes Observed by Magnetic Resonance Imaging in a Hamster Model of Transmissible Spongiform Encephalopathy: a Potential Biomarker of Prion Infection. J Mol Biomark Diagn 2:120. doi:10.4172/2155-9929.1000120

Copyright: © 2011 Baydack RS, et al. This is an open-access article distributed under the terms of the Creative Commons Attribution License, which permits unrestricted use, distribution, and reproduction in any medium, provided the original author and source are credited

scrapie brain homogenates. Magnetic resonance images were collected at 19; 33; 47; and 61 days post injection (dpi). At each time point a series of nine coronal images were collected (Figure 1). Differences were observed between infected hamsters and mock-infected or uninfected controls in slices five and six as early as the first time point (19 dpi).

Increases in T_2 relaxation time were observed in the hippocampus of infected animals in MRI slices five and six (Figure 2 and Figure 3, respectively). The pixel intensity on T_2 -maps reflects the T_2 relaxation time, which varies with specific experimental conditions (e.g. temperature). In order to compare images collected at different times, it was necessary to express the T_2 relaxation time in the region of interest (ROI) in relative terms, and to define the ROI according to the boundaries of the damage observed on the images. Contour plots were used to define the ROIs in individual animals, by identifying areas where T_2 relaxation time changed rapidly. In control and mock-infected hamsters, where contour plots did not identify affected regions, standard ROIs of a smaller size were used for comparison. Since minimal differences were observed in the thalamus between groups of hamsters at any time point, the T_2 relaxation time in that region of the brain was used as a correction factor to account for differences in experimental conditions during the collection of MR images: the mean T_2 relaxation time in the ROI was expressed as a percentage of that in the thalamus. Actual T_2 relaxation times in affected regions at 61 dpi were on the order of 70 ms in slice 5 and 90 ms in slice 6; in the thalamus, T_2 relaxation times measured in the low- to mid-fifties.

At 19 days post injection (dpi), scrapie-infected hamsters had a significantly different T_2 value compared to mock-infected hamsters injected with PBS, and uninfected control hamsters (Figure 2). The difference between the infected and control groups was significant ($p=0.0265$, ANOVA). At 33 dpi, the T_2 values of infected hamsters were significantly higher than those of mock-infected hamsters ($p=0.0004$).

The differences between infected and un-infected hamsters were more pronounced in MRI slice six at 47 and 61 dpi (Figure 3). At these time points, infected hamsters had significantly higher T_2 values than both mock-infected and control hamsters, while there were no significant differences between the latter two groups. At 33 dpi, there were significant differences between scrapie-infected hamsters and un-injected controls. Taking MRI slices five and six into consideration together, differences between infected hamsters and both uninfected controls and mock-infected hamsters were statistically significant at 33, 47, and 61 dpi; at 19 dpi, infected hamsters could be distinguished from controls only.

Histological changes in scrapie-infected hamsters

In order to explore the causes of scrapie-induced changes on

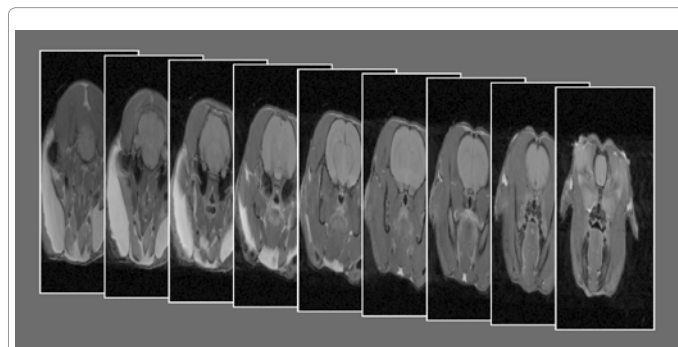


Figure 1: Images of nine coronal brain slices collected by Magnetic Resonance Imaging (MRI). Slices were numbered from posterior to anterior (left to right).

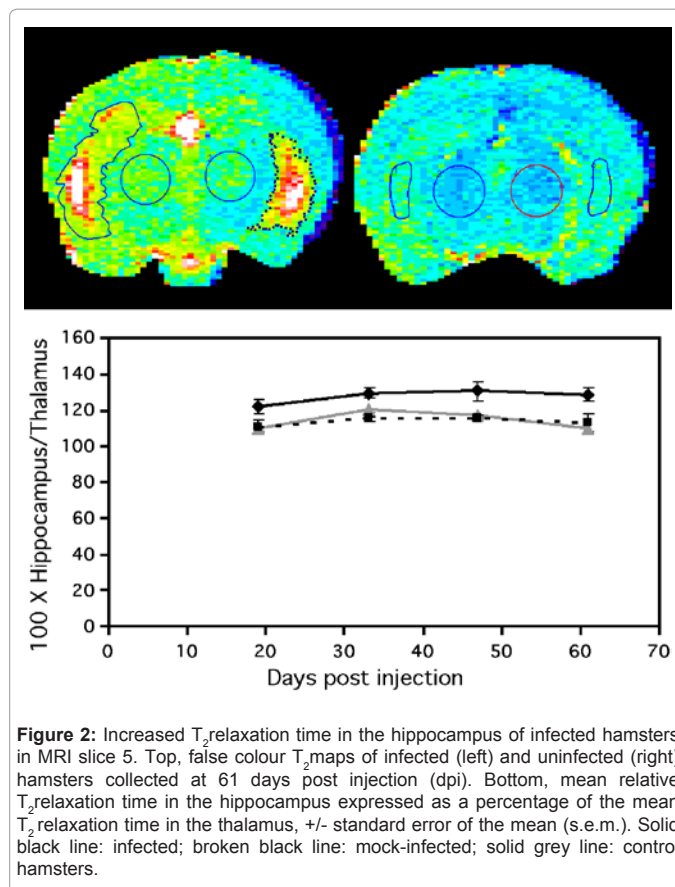


Figure 2: Increased T_2 relaxation time in the hippocampus of infected hamsters in MRI slice 5. Top, false colour T_2 -maps of infected (left) and uninfected (right) hamsters collected at 61 days post injection (dpi). Bottom, mean relative T_2 relaxation time in the hippocampus expressed as a percentage of the mean T_2 relaxation time in the thalamus, +/- standard error of the mean (s.e.m.). Solid black line: infected; broken black line: mock-infected; solid grey line: control hamsters.

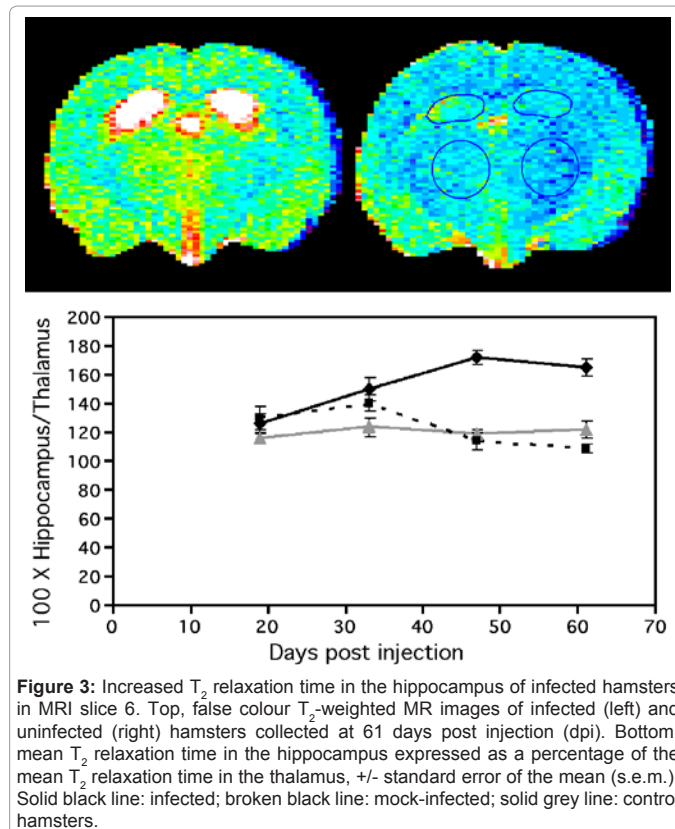


Figure 3: Increased T_2 relaxation time in the hippocampus of infected hamsters in MRI slice 6. Top, false colour T_2 -weighted MR images of infected (left) and uninfected (right) hamsters collected at 61 days post injection (dpi). Bottom, mean T_2 relaxation time in the hippocampus expressed as a percentage of the mean T_2 relaxation time in the thalamus, +/- standard error of the mean (s.e.m.). Solid black line: infected; broken black line: mock-infected; solid grey line: control hamsters.

MR images of hamster brains, different brain regions were examined at each time point for three histological hallmarks of prion disease: spongiform change; accumulation of PrP^{Sc}; and gliosis (Figure 4). The hippocampus was chosen, along with three regions where no obvious differences were observed between infected, mock-infected, and control hamsters: the cortex at the level of the thalamus; the thalamus; and the hypothalamus. All four of these regions are part of the lesion profile commonly used to evaluate spongiform change in rodents with prion disease. Qualitatively, the thalamus was the region most affected by histological changes, particularly spongiform change and PrP^{Sc} deposition. In order to make a more quantitative assessment, images of histological slides were evaluated using image processing software, allowing measurements of vacuolation, accumulation of PrP^{Sc}, and gliosis. Since mock-infected and control hamsters yielded similar results on MRI, they were assembled into a single “Uninfected” group for the purpose of histological examination.

A comparison between infected and uninfected hamsters shows differences in all three histological hallmarks of prion disease in the four regions of interest at 61 dpi (Figure 5). Significant differences in spongiform change were observed between infected and uninfected hamsters at 61 dpi in the thalamus, including the percentage of tissue covered by vacuoles ($p=0.0137$) and the total numbers of vacuoles ($p=0.0164$). There were also significant differences in anti-GFAP staining in both the cortex and the thalamus.

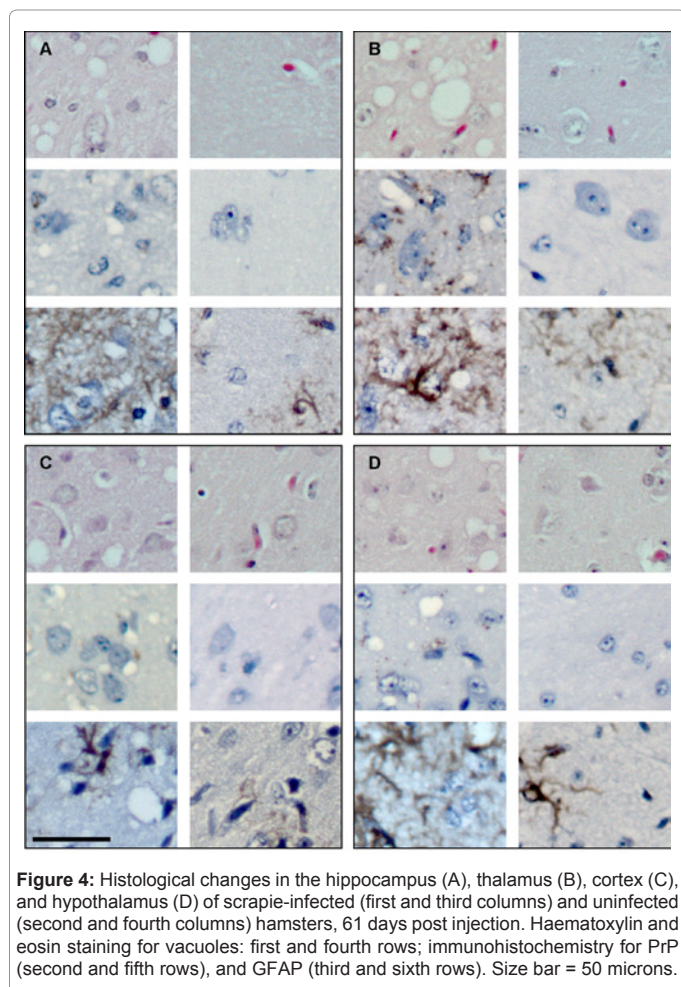


Figure 4: Histological changes in the hippocampus (A), thalamus (B), cortex (C), and hypothalamus (D) of scrapie-infected (first and third columns) and uninfected (second and fourth columns) hamsters, 61 days post injection. Haematoxylin and eosin staining for vacuoles: first and fourth rows; immunohistochemistry for PrP (second and fifth rows), and GFAP (third and sixth rows). Size bar = 50 microns.

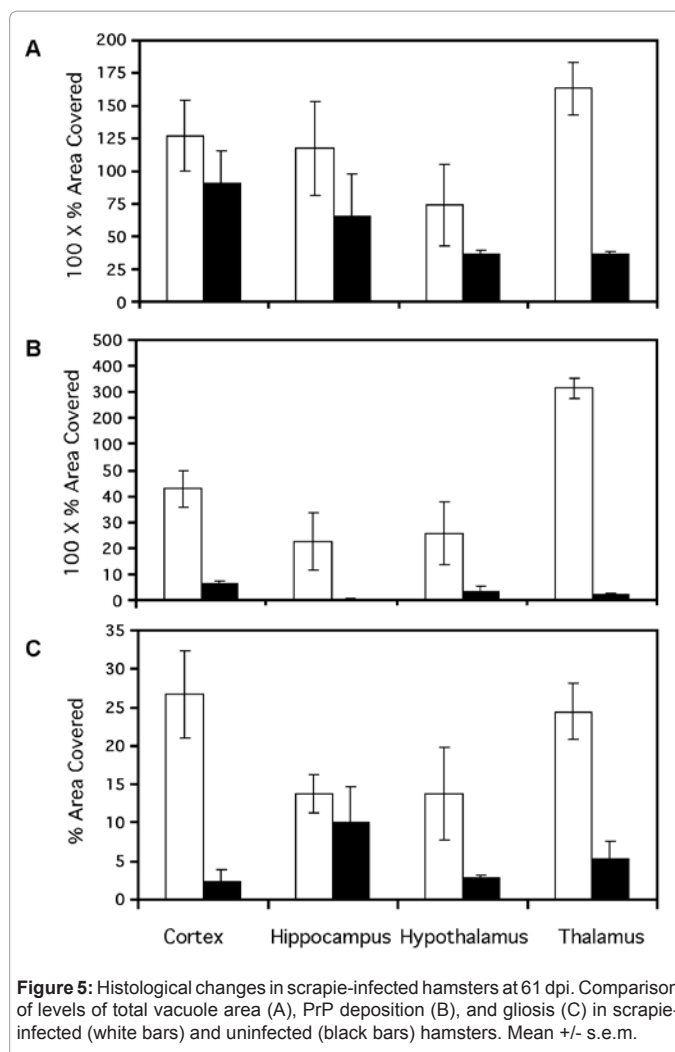


Figure 5: Histological changes in scrapie-infected hamsters at 61 dpi. Comparison of levels of total vacuole area (A), PrP deposition (B), and gliosis (C) in scrapie-infected (white bars) and uninfected (black bars) hamsters. Mean \pm s.e.m.

By examining the onset and progressing patterns of histological hallmarks of prion disease, we hoped to explain the differences observed on MR images. Beginning with spongiform change (Figure 6A), three of the regions of interest present similar curves: the cortex; the hippocampus; and the hypothalamus. In each case, vacuolation remains low in the earlier time points with a spike at 61 dpi; the levels observed in the hypothalamus remain lower than the other two regions throughout. In comparison, vacuolation in the thalamus is similar to that in the hypothalamus at the first time point, and then increases through the final two time points, making the thalamus the most highly vacuolated region at both 47 and 61 dpi. The curves of all four regions effectively parallel each other after the onset of significant changes; this seems to indicate that once spongiform change begins to occur, it appears at the same pace, regardless of brain region. Spongiform change cannot, however, be evaluated solely on the basis of the fraction of a brain section that is covered by vacuoles; the number of vacuoles present is also important. In the four brain regions studied, the curves representing area covered by vacuoles were effectively mirrored by those representing the number of vacuoles in a given area of tissue (Figure 7). In each case the increase in vacuole area, once initiated, was more rapid than that in number of vacuoles. Thus the total vacuole area increases not only with the addition of new vacuoles, but with the expansion of those vacuoles that were already present as well.

Although PrP^{Sc} deposition follows a similar pattern to that of spongiform change, it is not identical (Figure 6B). Once again, the cortex, hippocampus, and hypothalamus share almost identical curves, with no real increase over the first three time points before an increase at 61 dpi. In this case, the level of PrP^{Sc} in the cortex at 61 dpi is clearly higher than that in either the hippocampus or the hypothalamus. PrP^{Sc} levels in the thalamus of infected animals increased at the first time point, and continued to increase throughout the time course. This increase became exponential over the last time point (note the scale break in Figure 6B).

All four brain regions showed similar gliosis levels between 19 and 47 dpi, with an increase at 61 dpi. The cortex and thalamus showed a greater increase at the end of the time period studied, with the highest final gliosis measurements.

The thalamus showed the greatest changes in histology compared to the other regions studied. Moreover, the onset of the changes was earlier, and in a specific order (Figure 8). In the cortex, hippocampus, and hypothalamus, changes in histology were not seen until 61 dpi (Figure 8A-C).

In the thalamus (Figure 8D) an increase in PrP^{Sc} levels was evident as early as 33 dpi; increased vacuole levels were apparent at 47 dpi; while proliferation of glial cells appeared at 61 dpi.

Apparent diffusion coefficient magnetic resonance imaging

Since it was apparent that abnormalities observed on T₂ MR images appeared before histological changes, apparent diffusion coefficient (ADC) MR images were compared to T₂-maps (Figure 9). It was determined that regions with increased T₂ relaxation time (hyper-intensities in the hippocampus in slices 5 and 6) corresponded to increased ADC values, indicating that image abnormalities may be the result of fluid accumulation in the hippocampus. In infected hamsters at 61 dpi, ADC values in the hippocampus were greatest in slice 5 (1.21 x 10⁻³ mm²/s) and slice 6 (1.71 x 10⁻³ mm²/s). In control and mock-infected hamsters, the highest single ADC value in the hippocampus at 61 dpi was 8.85 x 10⁻⁴ mm²/s in slice 5 and 1.20 x 10⁻³ mm²/s in slice 6.

Discussion

In this study we were able to distinguish scrapie-infected hamsters from mock-infected and uninfected controls using MRI during the pre-clinical stage of disease. We also demonstrated that it is possible to follow disease progression longitudinally in individual animals, by imaging animals on successive time points. Furthermore, the differences observed in pre-clinical MR images did not correlate with the typical histological hallmarks of prion disease, and occurred earlier in the incubation period, potentially identifying a new marker for brain pathology. The fluid content of brain tissue appeared to increase in the hippocampus early in disease progression, as evidenced by changes in T₂ relaxation time and apparent diffusion coefficient observed by MRI.

Intra-cerebrally inoculated hamsters were differentiated from mock-infected and uninfected controls by statistically significant hyper-intensities in the hippocampus at 33, 47, and 61 dpi. All four of these time points were in the pre-clinical stage of disease; the documented incubation period of 263K scrapie in Syrian golden hamsters following i.c. infection is on the order of 68-71 dpi [8,9]. Although the 263K strain of scrapie is very fast acting, it was remarkable to find significant differences as early as we did. Abnormalities on MR images have previously been reported for prion diseases in both humans [12,14,20-22] and rodents [18,19,23], with variable results. In the case of the

human studies, all MRI scans were carried out during the symptomatic stage of disease. To our knowledge, only one rodent study has identified pre-clinical differences between infected and control animals, at 120 dpi using the 139A strain of scrapie in mice [19]. While it is difficult to compare disease stages in two different TSE strains and two different hosts, it seems apparent that the differences presented in the current study represent an earlier stage of disease: we observed changes at the one-quarter to one-third mark of the incubation period, compared to approximately the two-third mark in the previous study.

Our histological observations cannot explain the hyper-intensities found on T₂-weighted images, since those MR abnormalities precede histological changes, and since the regions most affected according to MRI and histology are not the same.

The changes observed by MRI in our study could not have been due to vacuolation or gliosis, since the MRI changes occurred at time points well before the onset of significant spongiform changes and gliosis in the regions investigated. In the infected hamsters, there was significant spongiform change only at 61 dpi, and in PrP^{Sc} deposition at 47 and 61 dpi in the thalamus; and in gliosis at 19 dpi in the hippocampus and at 61 dpi in both the cortex and the thalamus, as compared to uninfected controls. Thus the hippocampus, the region most affected according to MRI, did not have significant spongiform change over the

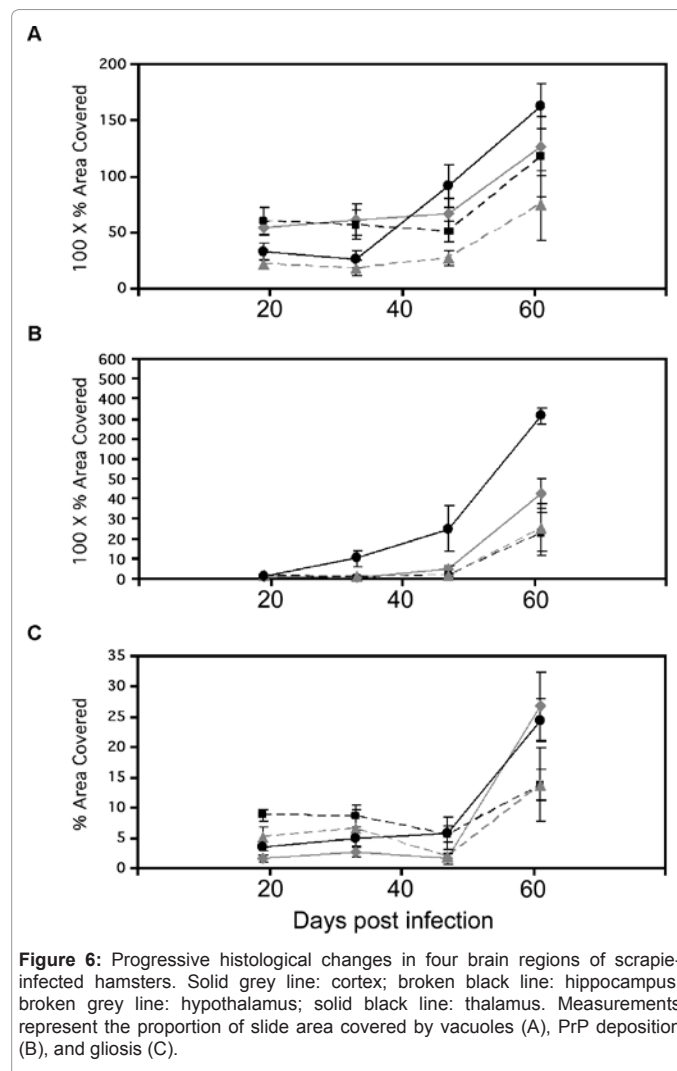


Figure 6: Progressive histological changes in four brain regions of scrapie-infected hamsters. Solid grey line: cortex; broken black line: hippocampus; broken grey line: hypothalamus; solid black line: thalamus. Measurements represent the proportion of slide area covered by vacuoles (A), PrP deposition (B), and gliosis (C).

course of the experiment, and only had slightly increased gliosis by the last time point. (61 dpi: Figure 6C).

The appearance of spongiform change, PrP^{Sc} deposition, and gliosis followed a common pattern in the hippocampus, cortex, and hypothalamus of 263K scrapie-infected hamsters: these results agree with previous studies involving the same scrapie and host strains and route of inoculation. Previous studies sequentially evaluated spongiform change and gliosis following i.c. infection in regions of the brain including those examined here [24,25]. The earliest observation of both pathologies occurred between 49 and 57 dpi [25], although only minor changes were observed at 52 dpi in the other study [24]. Masters et al report that from 49-57 dpi onward, the degree of spongiform change in the cortex and the hippocampus is greater than in the thalamus and the hypothalamus, while gliosis is more prevalent in the thalamus and the cortex [25]. These results support our findings. Two previous studies evaluating PrP^{Sc} distribution in the brains of infected hamsters between 7 and 65 dpi also support our results [26,27]. It was shown that PrP^{Sc} accumulated earliest and most significantly in the thalamus, beginning at 28-35 dpi, and that significant deposition in the cortex, hypothalamus, and hippocampus occurred only at 65 dpi

In a study carried out with μ MRI on mice infected with scrapie, clinical symptoms appeared (around 150 dpi), and severe neurological deficits were present by 180 dpi [19]. Hyper-intensities were observed in the septum, hippocampus, and cortex of infected mice, with corresponding increases in PrP^{Sc} deposition and gliosis, while spongiform change was not significant in these areas. A previous study using MR imaging on 263K scrapie-infected hamsters during the clinical stage of disease (74 dpi), compared the results to histological examination: neither spongiform change, gliosis nor PrP^{Sc} deposition correlated with MR changes [18].

T_2 relaxation time is determined by the relative mobility of water molecules. Biofluids are characterized by relatively long T_2 relaxation times, because of the high velocity of water molecules; dense, viscous fluids usually result in short T_2 relaxation times due to the reduced velocity of water molecules. We believe that the observed increase in T_2 relaxation time in the hippocampus of infected hamsters indicates an increase in fluid content. The correlation of increased ADC values with high T_2 relaxation times supports this conclusion. The apparent diffusion coefficient is a measure of the mobility of water molecules. High ADC values correspond to free movement of water, while low values indicate that water movement is restricted, for example by cell membranes. Therefore, long T_2 relaxation times and high ADC values observed in the hippocampus of infected hamsters would seem to indicate the accumulation of extracellular fluid, also known as vasogenic edema.

Cytotoxic edema is the result of accumulation of fluid inside cells, and is characterized by cellular swelling. Following initiation of swelling, individual oligodendrocytes [28] and neurons [29] mostly succumb to necrosis within 24 hours, while astrocytes begin to undergo necrosis after 24 hours [30]. Therefore, if cytotoxic edema occurred, it would have only a transient effect on ADC values, but it would result in swelling followed by necrosis of neurons as well as glial cells. While hypertrophy of glial cells has been documented in this disease model [31], a high degree of gliosis only occurs at about 80 dpi [24]. Because of this, we believe that the corresponding hyper-intensities on T_2 - and diffusion-weighted MR images are likely the result of vasogenic edema in the hippocampus of 263K scrapie-infected hamsters. In further support of this, breakdown of the blood-brain barrier, which is the cause of vasogenic edema [32], has been reported in experimental

prion disease [23,33], in both cases evaluated by MRI. Chung et al reported disruption of the blood-brain barrier during clinical scrapie in hamsters [23], while Brandner et al observed progressive break down specific to neural grafts over-expressing PrP^C in PrP null mice [33].

Increased expression of the water channels aquaporin-1 and -4 (AQP1 and AQP4) has been reported in cases of CJD, as well as in BSE-infected bovine-PrP transgenic mice [34]. In the case of the transgenic mice, AQP1 and AQP4 levels were elevated only at 270 dpi, when vacuoles and PrP^{Sc} deposits appeared. Expression of AQP4, the main water channel in the brain, is thought to be regulated through protein kinase C (PKC) and/or mitogen-activated protein kinase (MAPK) signaling pathways. Specifically, AQP4 mRNA and protein

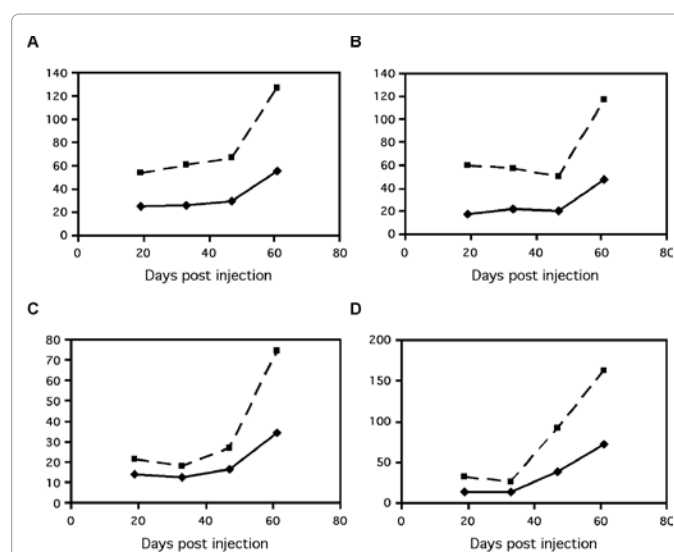


Figure 7: Relationship between total vacuole area and the number of vacuoles in the cortex (A); hippocampus (B); hypothalamus (C); and thalamus (D) of scrapie-infected hamsters. Scale: number of vacuoles/digital image (solid black line); 100 x percentage of image area covered by vacuoles (broken black line).

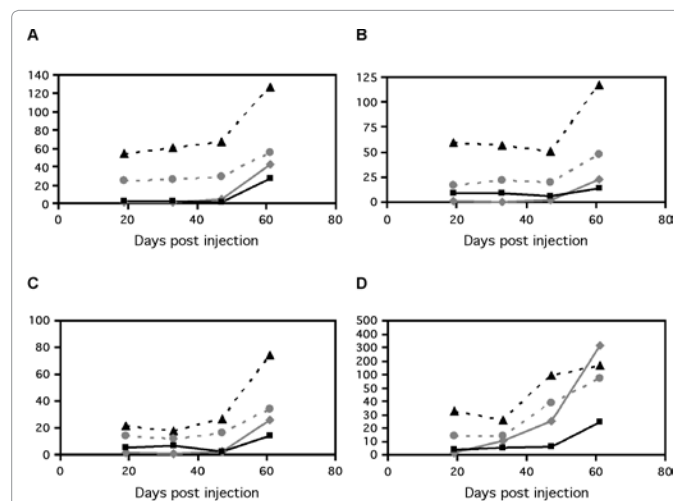


Figure 8: Patterns of histological changes in the cortex (A); hippocampus (B); hypothalamus (C); and thalamus (D) of scrapie-infected hamsters. Scale: 100 x percentage of image area covered by PrP (solid grey line) or vacuoles (broken black line); percentage of image area covered by gliosis (solid black line); number of vacuoles/digital image (broken grey line).

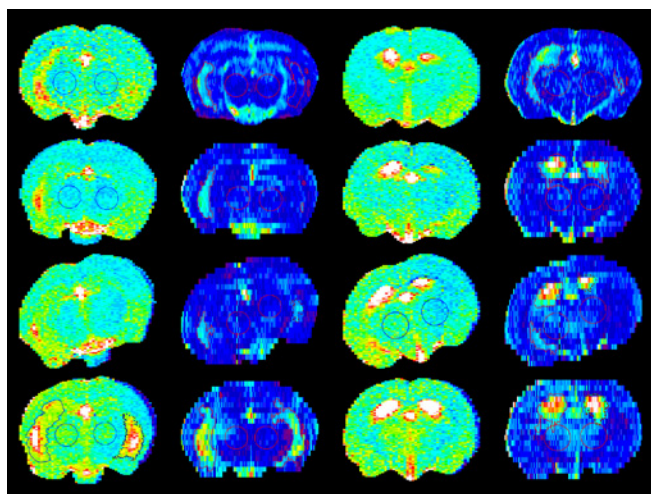


Figure 9: Comparison of T_2 maps and apparent diffusion coefficient (ADC) maps in the same scrapie-infected hamster between 19 and 61 dpi. First column: slice 5 T_2 maps; second column: slice 5 ADC maps; third column: slice 6 T_2 maps; fourth column: slice 6 ADC maps. Rows 1-4: images collected at 19, 33, 47, and 61 dpi, respectively.

levels are increased through a p38 MAPK-dependent pathway [35], and inhibited in a PKC-dependent manner [36]. In addition, PKC has been shown to inhibit the activity of AQP4 by phosphorylating it, causing a decrease in its permeability to water [37,38]. PrP^C has been implicated in cell signaling, including through both MAPK- [39,40] and PKC-dependent pathways [41]. The sequential activation of p38 MAPK has been demonstrated from 50 dpi onward in 263K scrapie-infected hamsters [42]. It is tempting to speculate that dysregulation of p38 MAPK and/or PKC signaling pathways due to a loss/modulation of normal PrP^C function may be responsible for the increased expression of AQP4 observed during the clinical stage of prion disease.

As a water channel, AQP4 is important in maintaining water homeostasis in the brain, and is therefore implicated in cerebral edema. AQP4 null mice have been evaluated in their response to both vasogenic and cytotoxic edema. The absence of AQP4 was associated with improved neurological outcome and reduced brain swelling in models of cytotoxic edema including water intoxication and ischemic stroke [43], and pneumococcal meningitis [44]. In contrast, AQP4 null mice fared worse than controls in models of vasogenic edema including staphylococcal brain abscess [45], and intraparenchymal fluid infusion, freeze-injury, and brain tumour [46]. These observations indicate that AQP4 is helpful in combating vasogenic cerebral edema, but detrimental in cases of cytotoxic edema. PrP^C expression is upregulated following focal cerebral ischemia [47], a model of cytotoxic edema, and PrP^C deletion leads to worsened outcome following ischemic brain injury [48,49]. This supports the theory that loss of PrP^C function late in prion disease pathogenesis results in increased AQP4 expression, since increased AQP4 expression would be detrimental following ischemic brain injury. We believe that the chronic edema reported in this study is vasogenic in nature [50].

We have demonstrated for the first time progressive increases in both T_2 relaxation time and apparent diffusion coefficient in the hippocampus of scrapie-infected hamsters beginning very early in disease progression. These MR image abnormalities are indicative of accumulation of fluid in the hippocampus, occurring earlier than any prion disease-associated histological changes. We speculate that

alterations in AQP4 expression previously reported during clinical disease [32] may result in initiation of edema, which may play a part in glial cell swelling and neuronal death. Confirmation of the exact role of edema in prion disease must await further studies.

Materials and Methods

Injections

Five-week-old Syrian golden hamsters were injected intracerebrally with 50 microlitres of 1% (w/v) 263 K scrapie brain homogenate in phosphate buffered saline (PBS), obtained from the TSE Resource Centre, Institute for Animal Health (Compton, Newbury, Berkshire, UK) as a stock 10% suspension. Mock-infected hamsters were injected with 50 microlitres of PBS only, and controls received no injection. Injections were performed into the right parietal region of the brain under isoflurane anaesthetic, using a needle fitted with a guard to prevent it from penetrating too deeply.

Magnetic Resonance Imaging

Beginning at 19 days post injection (dpi), hamsters underwent magnetic resonance imaging (MRI) every two weeks until either 47 or 61 dpi. Imaging was performed using a Bruker 7 Tesla scanner. Hamsters were enclosed in a custom-made holder, and breathing and temperature were monitored throughout imaging under isoflurane anaesthetic. A custom-made quadrature coil was used, and T_2 -weighted and diffusion weighted images were acquired using respiratory gating as a trigger for the Radio Frequency (RF) sequence. Nine coronal slices were collected, 1.7 mm thick and 2 mm apart. T_2 parameters: TR=1450 ms; TE=15 ms; 6 echoes (at multiple times of TE); field of view 3 x 3 cm; data matrix 256 x 128; 1 average. Diffusion-weighted imaging parameters (spin-echo sequence): TR=1200 ms; TE=40 ms; 1 echo; field of view 3 x 3 cm; data matrix 256 x 64. T_2 -maps were produced from T_2 -weighted data; apparent diffusion coefficient (ADC) maps were produced from diffusion-weighted data.

Collection of Tissues

Hamsters having undergone MRI were euthanized at 48 or 62 dpi by intra-cardiac injection of Euthanol. Each hamster brain was removed and frozen at -80°C for infrared microspectroscopic analysis, and for production of brain homogenate for subsequent infections. Hamsters to be examined histologically were euthanized in the same manner at 19, 33, 47, or 61 dpi. Upon removal, brains were fixed in formalin, dehydrated, and embedded in paraffin for sectioning.

Histological Examination

Paraffin-embedded sections 5-6 microns thick were examined for the histological hallmarks of prion disease. Sections were stained with hematoxylin and eosin for evaluation of spongiform change using standard procedures. Other sections were probed with anti-PrP or anti-GFAP (glial fibrillary acidic protein) antibodies according to the manufacturer's directions to evaluate PrP^{Sc} deposition and gliosis, respectively. Before immunohistochemistry for PrP, epitopes were exposed on sections by autoclaving with HCl. Monoclonal antibody 3F4 was used to identify PrP deposits, with visualization using a biotinylated goat anti-mouse secondary antibody and DAB with horseradish peroxidase. Polyclonal anti-GFAP antibody raised in rabbit was used to stain glial cells, using the same visualization method, substituting a goat anti-rabbit secondary antibody.

Quantification of Histological changes

Images of stained sections were acquired using a Leica light

microscope fitted with a digital camera. ImagePro software was used to quantify spongiform change, PrP^{Sc} deposition and glial cell staining in four selected regions of the brain: the hippocampus; the retrosplenial cortex; the thalamus; and the hypothalamus. For images of sections stained immunohistochemically, the software was used to create a template of the colour range identifiable as being immuno-stained. This template was then applied to all images, and a measurement, consisting of the percentage of the total image area that was covered by immunostaining, was produced. In the case of gliosis, the measurement was expressed as the raw percentage, whereas PrP^{Sc} deposition was expressed as 100 x % area covered.

In order to measure spongiform change, ImagePro software was used to evaluate potential vacuoles based on their size and shape. The size and shape restrictions were based on those set out by Sutherland et al. [51,52], except that vacuoles of a smaller size were included in this analysis (minimum of 8 square microns compared to 69). Potential vacuoles whose aspect ratios exceeded 3 or whose convex hull area to object area ratios exceeded 1.7 were eliminated. Before any measurements were collected or potential vacuoles were excluded, a series of image processing steps was applied to precisely define the boundaries of each object. The image was converted to greyscale and a Fast Fourier Transform was performed. A low-pass filter was then applied using Hanning filtering to attenuate high frequency information in the image, and an inverse Fourier Transform was executed. Finally, an intensity threshold was applied, eliminating lower intensity areas of the image, and leaving only potential vacuoles.

Statistical Analysis

MR images were processed using in-house developed software (Marevisi). Contour plots of T₂ relaxation time were created from the multi-echo data sets in order to identify regions that were consistently affected in infected hamsters.

In order to compare the mean T₂ relaxation time in the region identified (the hippocampus in two consecutive brain slices), in images collected at different times, this measurement was expressed as a percentage of the mean T₂ relaxation time in the thalamus of the same image. This region was chosen because minimal differences were observed in the thalamus between hamster groups at any of the four time points studied. In this way, the measurements being compared were corrected for differences in experimental conditions during MR image collection. At each of the four time points, an ANOVA was carried out to compare the corrected T₂ values in the hippocampus in the three hamster groups. In certain instances, comparison by ANOVA was not possible due to heterogeneity of variances between groups. In these cases, groups were compared using the Kruskal-Wallis test. ADC images were processed in the same manner.

For the purpose of comparison of histological hallmarks of prion disease, mock-infected and control hamsters were grouped together as a single group, called Uninfected, since MRI results were similar for both groups, and since neither were expected to show significant spongiform change or PrP^{Sc} deposition. At each time point, and for each histological characteristic being studied, two analyses were conducted: a series of t-tests comparing infected and uninfected groups in each of the four regions of interest; and an one way ANOVA comparing the four regions of interest in infected animals only.

References

- Collinge J (1997) Human prion diseases and bovine spongiform encephalopathy (BSE). *Hum Mol Genet* 6: 1699-1705.

- Pan KM, Baldwin M, Nguyen J, Gasset M, Serban A, et al. (1993) Conversion of alpha-helices into beta-sheets features in the formation of the scrapie prion proteins. *Proc Natl Acad Sci U S A* 90: 10962-10966.
- Pergami P, Jaffe H, Safar J (1996) Semipreparative chromatographic method to purify the normal cellular isoform of the prion protein in nondenatured form. *Anal Biochem* 236: 63-73.
- Oesch B, Westaway D, Walchli M, McKinley MP, Kent SB, et al. (1985) A cellular gene encodes scrapie PrP 27-30 protein. *Cell* 40: 735-746.
- Prusiner SB (1998) Prions. *Proc Natl Acad Sci U S A* 95: 13363-13383.
- Bruce ME, Will RG, Ironside JW, McConnell I, Drummond D, et al. (1997) Transmissions to mice indicate that 'new variant' CJD is caused by the BSE agent. *Nature* 389: 498-501.
- Collinge J, Sidle KC, Meads J, Ironside J, Hill AF (1996) Molecular analysis of prion strain variation and the aetiology of 'new variant' CJD. *Nature* 383: 685-690.
- Kimberlin RH, Cole S, Walker CA (1987) Pathogenesis of scrapie is faster when infection is intraspinal instead of intracerebral. *Microb Pathog* 2: 405-415.
- Kimberlin RH, Walker C (1977) Characteristics of a short incubation model of scrapie in the golden hamster. *J Gen Virol* 34: 295-304.
- Kimberlin RH, Walker CA (1978) Evidence that the transmission of one source of scrapie agent to hamsters involves separation of agent strains from a mixture. *J Gen Virol* 39: 487-496.
- Samman I, Schulz-Schaeffer WJ, Wohrle JC, Sommer A, Kretschmar HA, et al. (1999) Clinical range and MRI in Creutzfeldt-Jakob disease with heterozygosity at codon 129 and prion protein type 2. *J Neurol Neurosurg Psychiatry* 67: 678-681.
- Di RA, Molinari S, Stollman AL, Decker A, Yahr MD (1993) MRI abnormalities in Creutzfeldt-Jakob disease. *Neuroradiology* 35: 584-585.
- Hutzelmann A, Biederer J (1998) MRI follow-up in a case of clinically diagnosed Creutzfeldt-Jakob disease. *Eur Radiol* 8: 421-423.
- de Priester JA, Jansen GH, de KJ, Wilmink JT (1999) New MRI findings in Creutzfeldt-Jakob disease: high signal in the globus pallidus on T1-weighted images. *Neuroradiology* 41: 265-268.
- Murata T, Shiga Y, Higano S, Takahashi S, Mugikura S (2002) Conspicuity and evolution of lesions in Creutzfeldt-Jakob disease at diffusion-weighted imaging. *AJNR Am J Neuroradiol* 23: 1164-1172.
- Nitrini R, Mendonca RA, Huang N, LeBlanc A, Livramento JA, et al. (2001) Diffusion-weighted MRI in two cases of familial Creutzfeldt-Jakob disease. *J Neurol Sci* 184: 163-167.
- Mittal S, Farmer P, Kalina P, Kingsley PB, Halperin J (2002) Correlation of diffusion-weighted magnetic resonance imaging with neuropathology in Creutzfeldt-Jakob disease. *Arch Neurol* 59: 128-134.
- Chung YL, Williams A, Ritchie D, Williams SC, Changani KK, et al. (1999) Conflicting MRI signals from gliosis and neuronal vacuolation in prion diseases. *Neuroreport* 10: 3471-3477.
- Sadowski M, Tang CY, Aguinaldo JG, Carp R, Meeker HC, et al. (2003) In vivo micro magnetic resonance imaging signal changes in scrapie infected mice. *Neurosci Lett* 345: 1-4.
- Coulthard A, Hall K, English PT, Ince PG, Burn DJ, et al. (1999) Quantitative analysis of MRI signal intensity in new variant Creutzfeldt-Jakob disease. *Br J Radiol* 72: 742-748.
- Gertz HJ, Henkes H, Cervos-Navarro J (1988) Creutzfeldt-Jakob disease: correlation of MRI and neuropathologic findings. *Neurology* 38: 1481-1482.
- Zeidler M, Sellar RJ, Collie DA, Knight R, Stewart G, et al. (2000) The pulvinar sign on magnetic resonance imaging in variant Creutzfeldt-Jakob disease. *Lancet* 355: 1412-1418.
- Chung YL, Williams A, Beech JS, Williams SC, Bell JD, et al. (1995) MRI assessment of the blood-brain barrier in a hamster model of scrapie. *Neurodegeneration* 4: 203-207.
- Liberski PP, Alwasiak J (1983) Neuropathology of experimental transmissible spongiform encephalopathy (263 K strain of scrapie in golden Syrian hamsters). I. Standard pathology and development of lesions. *Neuropatol Pol* 21: 377-392.
- Masters CL, Rohwer RG, Franko MC, Brown P, Gajdusek DC (1984) The

- sequential development of spongiform change and gliosis of scrapie in the golden Syrian hamster. *J Neuropathol Exp Neurol* 43: 242-252.
26. Hecker R, Taraboulos A, Scott M, Pan KM, Yang SL, et al. (1992) Replication of distinct scrapie prion isolates is region specific in brains of transgenic mice and hamsters. *Genes Dev* 6: 1213-1228.
27. Jendroska K, Heinzel FP, Torchia M, Stowring L, Kretzschmar HA, et al. (1991) Proteinase-resistant prion protein accumulation in Syrian hamster brain correlates with regional pathology and scrapie infectivity. *Neurology* 41: 1482-1490.
28. Pantoni L, Garcia JH, Gutierrez JA (1996) Cerebral white matter is highly vulnerable to ischemia. *Stroke* 27: 1641-1646.
29. Garcia JH, Liu KF, Ho KL (1995) Neuronal necrosis after middle cerebral artery occlusion in Wistar rats progresses at different time intervals in the caudoputamen and the cortex. *Stroke* 26: 636-642.
30. Garcia JH, Liu KF, Yoshida Y, Chen S, Lian J (1994) Brain microvessels: factors altering their patency after the occlusion of a middle cerebral artery (Wistar rat). *Am J Pathol* 145: 728-740.
31. Liberski PP (1987) Astrocytic reaction in experimental scrapie in hamsters. *J Comp Pathol* 97: 73-78.
32. Heo JH, Han SW, Lee SK (2005) Free radicals as triggers of brain edema formation after stroke. *Free Radic Biol Med* 39: 51-70.
33. Brandner S, Isenmann S, Kuhne G, Aguzzi A (1998) Identification of the end stage of scrapie using infected neural grafts. *Brain Pathol* 8: 19-27.
34. Rodriguez A, Perez-Gracia E, Espinosa JC, Pumarola M, Torres JM, et al. (2006) Increased expression of water channel aquaporin 1 and aquaporin 4 in Creutzfeldt-Jakob disease and in bovine spongiform encephalopathy-infected bovine-PrP transgenic mice. *Acta Neuropathol (Berl)* 112: 573-585.
35. Arima H, Yamamoto N, Sobue K, Umenishi F, Tada T, et al. (2003) Hyperosmolar mannitol simulates expression of aquaporins 4 and 9 through a p38 mitogen-activated protein kinase-dependent pathway in rat astrocytes. *J Biol Chem* 278: 44525-44534.
36. Yamamoto N, Sobue K, Miyachi T, Inagaki M, Miura Y, et al. (2001) Differential regulation of aquaporin expression in astrocytes by protein kinase C. *Brain Res Mol Brain Res* 95: 110-116.
37. Zelenina M, Zelenin S, Bondar AA, Brismar H, Aperia A (2002) Water permeability of aquaporin-4 is decreased by protein kinase C and dopamine. *Am J Physiol Renal Physiol* 283: F309-F318.
38. Han Z, Wax MB, Patil RV (1998) Regulation of aquaporin-4 water channels by phorbol ester-dependent protein phosphorylation. *J Biol Chem* 273: 6001-6004.
39. Chen S, Mange A, Dong L, Lehmann S, Schachner M (2003) Prion protein as trans-interacting partner for neurons is involved in neurite outgrowth and neuronal survival. *Mol Cell Neurosci* 22: 227-233.
40. Lopes MH, Hajj GN, Muras AG, Mancini GL, Castro RM, et al. (2005) Interaction of cellular prion and stress-inducible protein 1 promotes neuritogenesis and neuroprotection by distinct signaling pathways. *J Neurosci* 25: 11330-11339.
41. Kanaani J, Prusiner SB, Diacovo J, Baekkeskov S, Legname G (2005) Recombinant prion protein induces rapid polarization and development of synapses in embryonic rat hippocampal neurons in vitro. *J Neurochem* 95: 1373-1386.
42. Lee HP, Jun YC, Choi JK, Kim JI, Carp RI, et al. (2005) Activation of mitogen-activated protein kinases in hamster brains infected with 263K scrapie agent. *J Neurochem* 95: 584-593.
43. Manley GT, Fujimura M, Ma T, Noshita N, Filiz F, Bollen AW, Chan P, Verkman AS (2000) Aquaporin-4 deletion in mice reduces brain edema after acute water intoxication and ischemic stroke. *Nat Med* 6: 159-163.
44. Papadopoulos MC, Verkman AS (2005) Aquaporin-4 gene disruption in mice reduces brain swelling and mortality in pneumococcal meningitis. *J Biol Chem* 280: 13906-13912.
45. Bloch O, Papadopoulos MC, Manley GT, Verkman AS (2005) Aquaporin-4 gene deletion in mice increases focal edema associated with staphylococcal brain abscess. *J Neurochem* 95: 254-262.
46. Papadopoulos MC, Manley GT, Krishna S, Verkman AS (2004) Aquaporin-4 facilitates reabsorption of excess fluid in vasogenic brain edema. *FASEB J* 18: 1291-1293.
47. Weise J, Crome O, Sandau R, Schulz-Schaeffer W, Bahr M, et al. (2004) Upregulation of cellular prion protein (PrP^C) after focal cerebral ischemia and influence of lesion severity. *Neurosci Lett* 372: 146-150.
48. Weise J, Sandau R, Schwarting S, Crome O, Wrede A, et al. (2006) Deletion of cellular prion protein results in reduced Akt activation, enhanced postischemic caspase-3 activation, and exacerbation of ischemic brain injury. *Stroke* 37: 1296-1300.
49. Spudich A, Frigg R, Kilic E, Kilic U, Oesch B, et al. (2005) Aggravation of ischemic brain injury by prion protein deficiency: role of ERK-1/2 and STAT-1. *Neurobiol Dis* 20: 442-449.
50. Verkman AS, Binder DK, Bloch O, Auguste K, Papadopoulos MC (2006) Three distinct roles of aquaporin-4 in brain function revealed by knockout mice. *Biochim Biophys Acta* 1758: 1085-1093.
51. Sutherland K, Rutovitz D, Bell JE, Ironside JW (1994) Evaluation of a novel application of image analysis. 378-381.
52. Sutherland K, Ironside JW (1994) Novel application of image analysis to the detection of spongiform change. *Anal Quant Cytol Histol* 16: 430-434.